MNRAS **000**, 1–14 (2016) Preprint 3 March 2016 Compiled using MNRAS LATEX style file v3.0

Super-Eddington growth of the first black holes

Edwige Pezzulli[1,2,3]⋆, Rosa Valiante[2] and Raffaella Schneider[2]
[1]*Dipartimento di Fisica, Universitá di Roma "La Sapienza", P.le Aldo Moro 2, 00185, Roma, Italy*
[2]*INAF/Osservatorio Astronomico di Roma, Via di Frascati 33, 00040 Monte Porzio Catone, Italy*
[3]*INFN, Sezione di Roma I, P.le Aldo Moro 2, 00185 Roma, Italy*

arXiv:1603.00475v1 [astro-ph.GA] 1 Mar 2016

1 March 2016

ABSTRACT
The assembly of the first super massive black holes (SMBHs) at $z \gtrsim 6$ is still a subject of intense debate. If black holes (BHs) grow at their Eddington rate, they must start from $\gtrsim 10^4\,M_\odot$ seeds formed by the direct collapse of gas. Here we explore the alternative scenario where $\sim 100\,M_\odot$ BH remnants of the first stars grow at super-Eddington rate via radiatively inefficient slim accretion disks. We use an improved version of the cosmological, data-constrained semi-analytic model GAMETE/QSODUST, where we follow the evolution of nuclear BHs and gas cooling, disk and bulge formation of their host galaxies. Adopting SDSS J1148+5251 (J1148) at $z = 6.4$ as a prototype of luminous $z \gtrsim 6$ quasars, we find that $\sim 80\%$ of its SMBH mass is grown by super-Eddington accretion, which can be sustained down to $z \sim 10$ in dense, gas-rich environments. The average BH mass at $z \sim 20$ is $M_{\rm BH} \gtrsim 10^4\,M_\odot$, comparable to that of direct collapse BHs. At $z = 6.4$ the AGN-driven mass outflow rate is consistent with the observations and the BH-to-bulge mass ratio is compatible with the local scaling relation. However, the stellar mass in the central 2.5 kpc is closer to the value inferred from CO observations. Finally, $\sim 20\%$ of J1148 progenitors at $z = 7.1$ have BH luminosities and masses comparable to ULAS J1120+0641, suggesting that this quasar may be one of the progenitors of J1148.

Key words:
quasars: supermassive black holes - galaxies: evolution - galaxies: high-redshift - galaxies: active - black hole physics - accretion, accretion discs

1 INTRODUCTION

High-redshift quasars are among the most luminous sources in the distant Universe. Their large luminosities ($L \sim 10^{47}$ erg/s) suggest that the powering mechanism of the strong radiative emission is the accretion of gas onto a Super Massive Black Hole (SMBH), with a mass $M_{\rm BH} \gtrsim 10^9 M_\odot$ settled in the center of the host galaxy (e.g. Fan et al. 2001, 2003; Willott et al. 2007). This phenomenon, in fact, can convert up to 30% of the energy in radiation, explaining the nature of this powerful emission (Shakura & Sunyaev 1973).

The most distant quasars are observed up to redshifts $z \sim 7$ (Mortlock et al. 2011), corresponding to a Universe younger than 1 Gyr old. How these SMBHs form and grow in such a short time is still an open question.

In the hierarchical scenario of structure formation, SMBHs are expected to grow via mergers with other BHs and gas accretion, starting from a less massive BH, generally referred to as BH seed. Hence, the formation and accretion history of SMBHs depend on the initial mass of BH seeds and on their formation epoch. The nature of the first BH seeds is still uncertain and different formation mechanisms have been proposed in the literature (see e.g. Volonteri 2010, and references therein):

(i) primordial black holes, with masses ranging from the Planck mass up to $10^5 M_\odot$ could have formed in the early Universe, well before galaxy formation (Khlopov et al. 2005);
(ii) remnants of the first generation of metal-poor stars, the so-called population III (Pop III) stars (see e.g. Bromm 2013 for a review), that can form to black holes of $\sim 100\,M_\odot$, at $z \sim 20$ (Madau & Rees 2001; Abel et al. 2002; Bromm et al. 2002; O'Shea & Norman 2007; Turk et al. 2009; Tanaka & Haiman 2009; Greif et al. 2012; Valiante et al. 2016);
(iii) gas-dynamical processes in massive environment can lead to the direct collapse of gas into a massive BH of $[10^4 - 10^6]$ M$_\odot$ (Bromm & Loeb 2003; Koushiappas et al. 2004; Begelman et al. 2006; Lodato & Natarajan 2006; Ferrara et al. 2014; Pacucci et al. 2015; Valiante et al. 2016);
(iv) stellar-dynamical processes allow BHs to form in nuclear clusters of second generation stars with masses $\sim [10^2 - 10^5] M_\odot$ (Devecchi & Volonteri 2009; Devecchi et al. 2010, 2012);
(v) gas-driven core-collapse of dense stellar clusters due to the rapid infall of gas with a mass comparable to that of the stellar cluster can lead to the formation of BHs of $\sim 10^3 M_\odot$ or larger (Davies et al. 2011; Lupi et al. 2014).

⋆ E-mail: edwige.pezzulli@oa-roma.inaf.it

© 2016 The Authors

In order to grow up to billion solar masses at $z \sim 6$, seed BHs must accrete gas at the Eddington rate almost uninterruptedly for several hundreds Myr, even if they start as "heavy seeds" of $[10^5 - 10^6]\,M_\odot$. Alternatively, short episodes of super-Eddington accretion have been suggested as a viable way to allow the efficient growth of SMBHs, especially if these start from "light seeds" of $\sim 100\,M_\odot$ (Haiman 2004; Yoo & Miralda-Escudé 2004; Shapiro 2005; Volonteri & Rees 2005, 2006; Pelupessy et al. 2007; Tanaka & Haiman 2009; Madau et al. 2014; Volonteri et al. 2015). In a recent numerical study, Lupi et al. (2015) show that, if a large reservoir of dense cold gas is available, a $M_{\rm BH} \sim 10^5 M_\odot$ can grow in a $\sim$ Myr timescale starting from a seed mass of $\sim 20 - 100\,M_\odot$, under the assumption of a slim accretion disk solution (Abramowicz et al. 1988). The slim disk solution, that we better describe in Section 2.3, represents an advective, optically thick flows that generalise the standard Shakura & Sunyaev solution (Shakura & Sunyaev 1973). In this model, the radiative efficiencies, that depend on the accretion rate, are low: the radiation is trapped and advected inward by the accretion flow (see however the recent simulations by Sądowski & Narayan 2016). In this scenario, the outflow has a negligible effect and the BH can accrete up to 80% – 100% of the gas mass available (Pacucci et al. 2015).

Indeed, there is observational evidence of mildly super-critical accretion (Kelly & Shen 2013; Page et al. 2014) in quasars at redshift up to ~ 7. In addition, recent numerical simulations aimed to study super-Eddington accretion onto a rapidly rotating BH (McKinney et al. 2014) and the energy, momentum and mass outflow rates from radiatively inefficient accretion discs (Sądowski et al. 2013) predict Eddington ratios $\eta_{\rm Edd} = L/L_{\rm Edd}$ up to 10, where $L_{\rm Edd}$ is the Eddington luminosity, defined as:

$$L_{\rm Edd} = \frac{4\pi G M_{\rm BH} m_p c}{\sigma_T} \simeq 3.3 \times 10^{10} \left(\frac{M_{\rm BH}}{10^6 M_\odot}\right) L_\odot \qquad (1)$$

with $M_{\rm BH}$ the central BH mass, m_p the proton mass, c the speed of light and σ_T the Thomson scattering cross section. Such a high ratio has been also invoked to explain the nature of ultraluminous X-ray sources (e.g. Middleton et al. 2013).

In this paper, we investigate the role of super-Eddington accretion in the formation of the first SMBHs at redshift $z \sim 6$, with the aim to understand what are the environments where it can occur and discuss the implications for the coevolution of the SMBHs and their host galaxies at high redshifts. We base our analysis on the data-constrained semi-analytical model GAMETE/QSODUST that allows to simulate a large number of hierarchical histories of a quasar host dark matter halo, following the star formation history, chemical evolution and nuclear black hole growth in all its progenitor galaxies. The model has been first successfully used to investigate the properties of the $z = 6.4$ quasar SDSS J1148+5251 by Valiante et al. (2011, 2012), applied to a sample of quasars at $5 < z < 6.4$ by Valiante et al. (2014) and more recently used to investigate the relative importance of light and heavy seeds in the early growth of high-z SMBHs under the assumption of Eddington-limited accretion (Valiante et al. 2016). Here we present an improved version of the model, that has been modified to follow gas cooling, disk and bulge formation, and BH gas accretion in all the progenitor systems of a $z = 6.4$ quasar, using SDSS J1148+5251 (hereafter J1148) as a prototype for the general class of luminous high-redshift quasars.

The paper is organized as follows. In Section 2 we introduce the model, describing assumptions and physical prescriptions. In Section 3 we present the results. Finally, a discussion and the main conclusions are given in Section 4.

2 THE MODEL

In this section we provide a brief summary of the original GAMETE/QSODUST model (referring the readers to Valiante et al. 2011, 2012, 2014 for a more detailed description) and we present the new features that have been implemented for the present study.

We reconstruct 30 independent merger histories of a dark matter halo at redshift 6.4 assumed to be the host of J1148. We adopt a Navarro Frenk & White (1995, NFW) density profile with a mass of $M_{\rm h} = 10^{13} M_\odot$, within the range supposed to host high-z bright quasars (Volonteri & Rees 2006; Fan et al. 2004) and simulate its hierarchical history using a binary Monte Carlo merger tree algorithm based on the Extended Press-Schechter theory (Lacey & Cole 1993).

The code follows the time evolution of the mass of gas, stars, metals and dust in a 2-phase ISM inside each progenitor galaxy (see also de Bennassuti et al. 2014), taking into account chemical enrichment from Asymptotic Giant Branch (AGB) stars and Supernovae (SNe), which inject dust and metals into the ISM, grain destruction by SN shocks and grain growth in dense molecular clouds. Energy-driven outflows, powered by both AGN and SN feedback, are considered in the model: the energy released by the BH accretion process and SN explosions couples with the gas and can unbind a huge amount of interstellar gas (Silk & Rees 1998). Although the physical mechanisms that trigger these galaxy-scale winds are still controversial, the model predicts mass ejection rates comparable to the observed ones (Maiolino et al. 2012; Valiante et al. 2012; Cicone et al. 2015).

Following Valiante et al. (2011, 2016) we focus our study on one of the most distant and best studied quasar, J1148, discovered at redshift $z \simeq 6.4$ (Fan et al. 2003). The observationally inferred properties of this quasar are reported in Table 1. These are used to calibrate the model by fixing the adjustable free parameters shown in Table 2, as described below.

In what follows, we discuss the new features of the code, namely: (*a*) the formation of the disk via gas cooling; (*b*) the formation of the bulge via major mergers; (*c*) bursted and quiescent star formation both in the disk and in the bulge; (*d*) the BH seeding prescription; (*e*) the BH growth via accretion and coalescences, considering also the recoil velocities that can be generated by the product of the merging pair due to asymmetric gravitational wave emission; (*f*) SNe and AGN feedback, responsible of galactic-scale winds.

We adopt a Lambda cold dark matter (ΛCDM) cosmology with parameters $\Omega_m = 0.314$, $\Omega_\Lambda = 0.686$, $h = 0.674$ (Planck Collaboration et al. 2014), so that the Hubble time at redshift 6.4 is 851 Myr. The difference with the cosmological parameters adopted in previous works (Valiante et al. 2011, 2014) is mainly the larger value of σ_8 (Planck $\sigma_8 = 0.834$, WMAP7 $\sigma_8 = 0.761$), which implies an increased power at small scales, leading to a larger number of progenitor systems at high redshifts.

2.1 Gas cooling

In each newly virialized dark matter halo with mass M_h, the initial gas mass is assumed to be the cosmic baryon fraction $M_{\rm diff} = (\Omega_{\rm b}/\Omega_{\rm m})\,M_h$. We suppose this gas to be all in the diffuse phase, i.e.

Table 1. Observed and inferred properties of the quasar SDSS J1148+5251. The black hole mass, $M_{\rm BH}$, is estimated from the Mg_{II} doublet and the $\lambda = 3000$ Å continuum (De Rosa et al. 2011). The mass of molecular gas, $M_{\rm H_2}$, and the dynamical mass, $M_{\rm dyn}\sin^2 i$, have been estimated from CO observations (see Valiante et al. 2014 for more details). The star formation rate, SFR, has been computed from the far-infrared (FIR) luminosity using the Kennicutt relation (see Section 3 fore further details). The value of $L_{\rm FIR}$ and $M_{\rm dust}$ have been computed by Valiante et al. (2011, 2014). The bolometric luminosity $L_{\rm bol}$ is estimated from the observed flux at 1450 Å (Fan et al. 2003) using the bolometric correction by Richards et al. (2006).

z	$M_{\rm BH}\,[10^9 M_\odot]$	$M_{\rm H2}\,[10^{10} M_\odot]$	$M_{\rm dyn}\sin^2 i\,[10^{10} M_\odot]$	$L_{\rm FIR}\,[10^{13} L_\odot]$	$L_{\rm bol}\,[10^{14} L_\odot]$	SFR $[10^3 {\rm M}_\odot/{\rm yr}]$	$M_{\rm dust}\,[10^8 M_\odot]$
6.42	4.9 ± 2.5	2.3 ± 1.9	3.4 ± 1.3	2.2 ± 0.33	1.36 ± 0.74	2.0 ± 0.5	$3.4^{+1.38}_{-1.54}$

pressure-supported, and to follow an isothermal density profile ρ_g defined as:

$$\rho_g(r) = \frac{M_{\rm diff}}{4\pi R_{\rm vir} r^2}, \tag{2}$$

where $R_{\rm vir}$ is the virial radius of the dark matter halo. The hot diffuse gas gradually cools providing the reservoir of cold gas out of which stars form. The gas cooling processes strongly depend on the temperature and chemical composition of the gas.

In dark matter halos with virial temperature $T_{\rm vir} < 10^4\,K$, referred to as mini-halos, the primordial gas can cool only through H_2 roto-vibrational transitions (Haiman et al. 1996). As the gas becomes progressively enriched in heavy elements, other molecular species can contribute to cooling and collisionally excited metal fine-structure lines, mostly OI, CII can provide additional cooling pathways. Here we only consider the contribution of H_2, OI and CII cooling using metallicity dependent tabulated cooling functions, $\Lambda(T_{\rm vir}, Z)$, computed as described in Appendix A of Valiante et al. (2016) but we neglect the effect of H_2 photo-dissociation by Lyman-Werner photons. We will return to this point in Section 3.

In dark matter halos with virial temperatures $T_{\rm vir} \geq 10^4$K, referred to as Lyman-α cooling halos, the temperature is high enough to excite atomic transitions, allowing the primordial gas to cool through hydrogen Lyman-α line emission. In this regime, we use metallicity-dependent tabulated cooling functions presented by Sutherland & Dopita (1993).

The time scale for gas cooling, $\tau_{\rm cool}$, is defined as:

$$\tau_{\rm cool} = \frac{3}{2}\frac{\mu m_p \kappa_B T_{\rm vir}}{\rho_g(r_{\rm cool})\Lambda(T_{\rm vir}, Z)}, \tag{3}$$

where κ_B is the Boltzmann constant, μ is the mean molecular weight and $r_{\rm cool}$ is the cooling radius and it is obtained by assuming that the cooling time is equal to the halo dynamical time $t_{\rm dyn} = R_{\rm vir}/v_{\rm DM}$, where $v_{\rm DM}$ is the dark matter (DM) halo circular velocity:

$$r_{\rm cool} = \left[\frac{t_{\rm dyn}\, M_{\rm diff}\, \Lambda(T_{\rm vir}, Z)}{6\pi\,\mu m_p\, \kappa_B T_{\rm vir}\, R_{\rm vir}^2}\right]^{1/2}. \tag{4}$$

Then, the gas cooling rate can be computed[1] as:

$$\dot{M}_{\rm cool} = 4\pi\rho_g(r_{\rm cool}) r_{\rm cool}^2 \frac{dr_{\rm cool}}{dt} = \frac{M_{\rm diff}}{2R_{\rm vir}}\frac{r_{\rm cool}}{t_{\rm dyn}}. \tag{5}$$

[1] Note that if $r_{\rm cool} > R_{\rm vir}$ we assume that the gas never reaches hydrostatic equilibrium and it is immediately available to star formation (De Lucia et al. 2010).

2.2 Disk and bulge formation

Along the hierarchical history of the final DM halo, we define major (minor) halo-halo merger events as those with halo mass ratio $\mu = M_{\rm halo,1}/M_{\rm halo,2}$ (with $M_{\rm halo,1} \leq M_{\rm halo,2}$) larger (lower) than $\mu_{\rm thr} = 1/4$ (Barausse 2012). In quiescent evolution (i.e. no encounters with other galaxies), the cold gas settles on a rotationally-supported disk, because of the conservation of angular momentum, and can start to form stars. The disk, composed of gas and stars, can be disrupted by a major merger and a spherical bulge is expected to form in this event. Minor mergers, instead, are not expected to destroy the disk but may help the growth of the bulge by disk instabilities (Naab & Burkert 2003; Bournaud et al. 2005).

In our model, major mergers are supposed to destroy both the gaseous and stellar disk components of the newly-formed galaxy, adding the stars and gas to the central bulge. Minor mergers do not contribute to the transfer of matter between the disk and bulge, and thus lead to the formation of a new galaxy with disk and bulge masses that are the sum of the two progenitors ones.

We consider a self-gravitating disk, with an exponential gas surface density profile, $\Sigma_{\rm d}$, defined as (Mo et al. 1998):

$$\Sigma_{\rm d}(r) = \Sigma_{\rm d}(0)\, e^{-r/R_{\rm d}}, \tag{6}$$

where $R_{\rm d}$ is the scale radius of the gaseous disk and $\Sigma_{\rm d}(0)$ is the central surface densities of the gas. For the stellar component of the disk, we adopt the same density profile with the same scale radius $R_{\rm d}$. Following Mo et al. (1998) we define the scale radius as,

$$R_{\rm d} = \frac{1}{\sqrt{2}}\left(\frac{j_{\rm d}}{m_{\rm d}}\right)\lambda R_{\rm vir}\frac{1}{\sqrt{f_{\rm c}}} f_{\rm R}(\lambda, c, m_{\rm d}, j_{\rm d}), \tag{7}$$

where $j_{\rm d} = J_{\rm d}/J$ is the ratio between the disk angular momentum and that of the halo, $m_{\rm d} = M_{\rm d}/M_{\rm h}$ is the disk mass (stars+gas) fraction over the halo mass. From the conservation of the specific angular momentum we assume $j_{\rm d}/m_{\rm d} = 1$. The spin parameter λ is considered to be constant and equal to 0.05, the mean value adopted by Mo et al. (1998).

The factors $f_{\rm c}$ and $f_{\rm R}$ take into account the correction to the total energy of the halo resulting from the NFW density profile and the gravitational effect of the disk, and are computed following the prescription given by Mo et al. (1998). The factor $f_{\rm c}$ depends on the concentration parameter c, that we assume to be constant and equal to $c = 1$[2]:

[2] Unfortunately, numerical studies of the concentration parameter of dark matter halos spanning the mass and redshift range relevant for the present study are not available. Extrapolating the results of Muñoz-Cuartas et al. (2011), we adopt a constant value of $c = 1$. At a fixed halo mass, BH growth would be favoured in more concentrated halos, that are characterized by a larger mass and circular velocity in the inner regions (Mo et al. 1998).

$$f_c = \frac{c}{2}\frac{1-1/(1+c)^2-2\ln(1+c)/(1+c)}{[c/(1+c)-\ln(1+c)]^2}. \quad (8)$$

The factor f_R is computed as,

$$f_R = 2\left[\int_0^\infty e^{-u}u^2\frac{v_c(R_d u)}{v_c(R_{vir})}\right]^{-1}, \quad (9)$$

where $v_c(r)$ is the total rotation velocity of the system,

$$v_c^2(r) = v_d^2(r) + v_b^2(r) + v_{DM}^2(r). \quad (10)$$

Here v_b is the circular velocity of the bulge, v_{DM} is the circular velocity of the DM halo and v_d is the circular velocity of the thin, exponential disk,

$$v_d^2 = \pi G \Sigma_0 x^2[I_0(x/2)K_0(x/2) - I_1(x/2)K_1(x/2)], \quad (11)$$

where $x = r/R_d$ and I_α, K_α are the modified Bessel functions of the first and second type, respectively and $\Sigma_0 = \Sigma(0)_d + \Sigma(0)_d^\star$ is the sum of the gas and stellar central ($r = 0$) surface densities.

For the bulge component, we assume that the gas density profile $\rho_b(r)$ is described as (Hernquist 1990),

$$\rho_b(r) = \frac{M_b}{2\pi}\frac{r_b}{r(r+r_b)^3}, \quad (12)$$

where the scale radius, r_b, is computed as $r_b = R_{eff}/1.8153$ (Hernquist 1990), and the effective radius R_{eff}[3], depends on the gas and stellar masses in the bulge (Shen et al. 2003):

$$\log(R_{eff}/\mathrm{kpc}) = 0.56\log(M_b + M_b^\star) - 5.54. \quad (13)$$

We adopt the same density profile for the stellar component in the bulge.

The velocity profile of the bulge, computed through the Poisson equation is

$$v_b^2 = \frac{Gr(M_b + M_b^\star)}{(r_b + r)^2}. \quad (14)$$

We assume that the halo responds adiabatically to the gradual build up of the disk and bulge, maintaining the spherical symmetry during the contraction. Thus, the angular momentum is conserved during the collapse from a mean initial radius r_i to a radius r ($< r_i$), so that:

$$M_f(r)r = M(r_i)r_i, \quad (15)$$

where $M(r_i)$ is the mass of DM enclosed in r_i obtained integrating the NFW density profile and $M_f(r)$ is the total final mass within a radius r:

$$M_f(r) = M_{d,t}(r) + M_{b,t}(r) + (1 - f_{gal})M(r_i), \quad (16)$$

where $M_{d,t}(r)$ and $M_{b,t}(r)$ are the total disk and bulge masses (star and gas) enclosed within a radius r, obtained by integrating eqs. (6) and (12), and $f_{gal} = [M_{d,t} + M_{b,t}]/M_h$ is the fraction of the total mass in the disk and bulge.

[3] R_{eff} is the effective radius of the isophote enclosing half the light.

Table 2. The calibrated values of the adjustable parameters of the reference model.

	Free parameters	values
$\epsilon_d^\star$	quiescent star formation efficiency	0.083
β	BH accretion efficiency	0.03
ϵ_{AGN}	AGN-feedback efficiency	1.5×10^{-3}

The velocity curve of the perturbed DM halo is then,

$$v_{DM}^2(r) = [G(M_f(r) - M_{d,t}(r) - M_{b,t}(r)]/r. \quad (17)$$

Following these prescriptions we model the formation and evolution of disk and bulge components in each halo along the reconstructed merger histories.

2.2.1 *Star formation rate*

Hydrodynamical simulations suggest that merging events, major mergers in particular, can trigger bursts of star formation in the central regions as a consequence of the tidal forces produced by galaxy-galaxy interactions (Mihos & Hernquist 1994; Springel 2000; Cox et al. 2008).

Since starbursts are confined in the very central region of the galaxy, we assume a quiescent mode of star formation in the disk while bursts are triggered in the bulge when a major merger occurs. The star formation rate (SFR) in the disk is described as,

$$\dot{M}_d^\star = \epsilon_d^\star\frac{M_d,}{\tau_d} \quad (18)$$

where M_d is the gas mass in the disk, $\tau_d = 3R_d/v_c(3R_d)$ is the dynamical time of the disk evaluated at the peak of the circular velocity profile (Mo et al. 1998), R_d is the disk scale radius defined in eq. 7 and $\epsilon_d^\star$ is an adjustable free parameter representing the star formation efficiency in the disk. In our reference model, $\epsilon_d^\star = 0.083$ (see Table 2).

Similarly, the SFR in the bulge is computed as,

$$\dot{M}_b^\star = \epsilon_b^\star\frac{M_b}{\tau_b}, \quad (19)$$

where M_b is the gas mass in the bulge, $\tau_b = R_{eff}/v_c(R_{eff})$ is the dynamical time of the bulge and the effective radius R_{eff} is defined in eq. 13 above. We assume that in absence of merger events, the star formation efficiency in the bulge is equal to that of the disk, $\epsilon_b^\star = \epsilon_d^\star$. When a merger event occurs, the star formation efficiency increases as a consequence of the destabilizing effect of the interaction, and we adopt the following scaling relation:

$$\epsilon_b^\star = \epsilon_d^\star\, f(\mu), \quad (20)$$

with $f(\mu) = \max[1, 1 + 2.5\,(\mu - 0.1)]$, so that mergers with $\mu \leq 0.1$ do not trigger starbursts. With the adopted scaling relation, the starburst efficiency in the reference model is $0.083 \leq \epsilon_b^\star \leq 0.27$, consistent with the range of values found by means of hydrodynamical simulations of merging galaxy pairs (Cox et al. 2008) and adopted by other studies (Menci et al. 2004; Valiante et al. 2011).

2.3 Black hole growth and feedback

2.3.1 BH seeds

We assume BH seeds to form only as remnants of first (Pop III) stars. In fact, our main aim is to investigate if SMBHs can form by super-Eddington accretion starting from "light" seeds at high redshift. Although the initial mass function of Pop III stars is still very uncertain, the most recent numerical simulations suggest a characteristic mass of a few hundreds of solar masses at $z \sim 25$, that progressively shifts to a few tens of solar masses at lower redshifts (Hirano et al. 2015). For simplicity, here we do not consider the redshift modulation of the characteristic mass and we plant a BH seed with a mass of $M_{\rm seed} = 100\,M_\odot$ in each newly-virialized halo with a metallicity $Z < Z_{\rm cr} = 10^{-4} Z_\odot$, above which the effects of dust and metal line cooling allow the gas to fragment, reducing the characteristic mass to values comparable to those found in local stellar populations (Schneider et al. 2002, 2003, 2012; Omukai et al. 2005).

2.3.2 BH accretion

Once formed, the BH accretes gas from the surrounding medium. The correlation between the mass of central SMBH and the bulge mass or velocity dispersion (Magorrian et al. 1998; Richstone et al. 1998, see Kormendy & Ho 2013 and references therein) and the small scale on which the accretion takes place, suggest that the accretion onto the central black hole should be fuelled by the cold gas present in the bulge.

The collapse of material onto the central BH in a galaxy is triggered by both merger-driven infall of cold gas, which loses angular momentum due to galaxy encounters, and quiescent accretion, assuming that the accretion rate is proportional to the cold gas mass in the bulge,

$$\dot{M}_{\rm accr} = \frac{f_{\rm accr} M_{\rm b}}{\tau_{\rm b}}, \tag{21}$$

where, similarly to eq. (20), the accretion efficiency is expressed as,

$$f_{\rm accr} = \beta\, f(\mu), \tag{22}$$

where β is an adjustable free parameter. In our reference model, $\beta = 0.03$ (see Table 2), so that the efficiency of BH accretion is about $\sim 1/3$ of the efficiency of star formation in the bulge.

Thus, the mass growth rate is,

$$\dot{M}_{\rm BH} = (1 - \epsilon_r)\dot{M}_{\rm accr}, \tag{23}$$

where the radiative efficiency ϵ_r is defined as,

$$\epsilon_r = \frac{L_{\rm bol}}{\dot{M}_{\rm accr}\, c^2}, \tag{24}$$

with $L_{\rm bol}$ being the bolometric luminosity emitted by the accretion process. At high accretion rates, the Shakura & Sunyaev (1973) model of BH growth through a thin disk, where all the heat generated by viscosity is immediately radiated away, is incorrect. Instead, it is possible to use the optically thick, slim accretion disk solution, that is characterized by low radiative efficiencies (Abramowicz et al. 1988).

The bolometric luminosity, $L_{\rm bol}$, is computed starting from the numerical solutions of the relativistic slim accretion disk equations obtained by Sądowski (2009), adopting the fit presented by Madau et al. (2014):

$$\frac{L_{\rm bol}}{L_{\rm Edd}} = A(a)\left[\frac{0.985}{\dot{M}_{\rm Edd}/\dot{M}_{\rm accr} + B(a)} + \frac{0.015}{\dot{M}_{\rm Edd}/\dot{M}_{\rm accr} + C(a)}\right], \tag{25}$$

where the Eddington accretion rate is defined as $\dot{M}_{\rm Edd} \equiv 16\, L_{\rm Edd}/c^2$ and $A(a)$, $B(a)$ and $C(a)$ are functions of the BH spin parameter a,

$$A(a) = (0.9663 - 0.9292a)^{-0.5639}, \tag{26}$$

$$B(a) = (4.627 - 4.445a)^{-0.5524}, \tag{27}$$

$$C(a) = (827.3 - 718.1a)^{-0.7060}. \tag{28}$$

The slim accretion disk model represented by eq. (25) predicts that even when the accretion rate is super-Eddington, with $1 \lesssim \dot{M}_{\rm accr}/\dot{M}_{\rm Edd} \lesssim 100$, the disk luminosity remains only mildy super-Eddington, with $L_{\rm bol} \lesssim (2-4)\, L_{\rm Edd}$. In fact, in this regime a large fraction of the energy generated by viscosity does not have the time to be radiated away and is instead advected into the black hole. As a result, the radiative efficiency is very small, with $0.002 \lesssim \epsilon_r \lesssim 0.05$, almost independently of the value of the BH spin parameter (see Figure 1 in Madau et al. 2014. Conversely, when the accretion rate is sub-Eddington, the radiative efficiency increases reaching an almost constant value which depends on the BH spin, as in the standard think disk solution, with $\epsilon_r \lesssim 0.05$ for $a = 0$ and $\epsilon_r \lesssim 0.3$ for $a = 0.98$.

Here we do not describe the time evolution of the BH spin parameter and we simply assume that the module of the spin vector a is randomly extracted from a uniform distribution (Tanaka & Haiman 2009; Barausse 2012).

2.3.3 BH mergers

In halo merging events, we assume that the two nuclear BHs coalesce with the same timescale of their host halos. However, in minor mergers (with $\mu < \mu_{\rm thr} = 1/4$, see Section 2.2) only the largest of the two progenitors BHs can settle in the centre of the new halo potential well, surviving as a nuclear BH, while the smaller one ends up as a satellite.

During the BH merger, the newly formed BH receives a large center-of-mass recoil due to the net linear momentum carried by the asymmetric gravitational waves emission (Campanelli et al. 2007; Schnittman et al. 2008; Baker et al. 2008). The recoil (or kick) velocity of the coalesced binary depends on the mass ratio of the merging pair and on the amplitude and orientation of the spin vectors of the two BHs. Here we follow the parametrization presented by Tanaka & Haiman (2009) and - for each merger event - we compute the kick velocity as a function of the BH mass ratio assuming the spin vectors to be randomly oriented. The average kick velocities increase with the mass ratio of the merging pair, $q = M_{\rm BH,1}/M_{\rm BH,2}$ (with $M_{\rm BH,1} \le M_{\rm BH,2}$). For strongly unequal mass mergers, with $0.01 \lesssim q \lesssim 0.1$, we find $\langle v_{\rm kick}\rangle = 1 - 100$ km/s, whereas for larger mass ratios, with $0.1 \lesssim q \lesssim 1$, the kicks can be very strong, with velocities $\langle v_{\rm kick}\rangle = 100 - 1000$ km/s.

We then compare the kick velocity with the circular velocity at the radius of influence of the BH, $R_{\rm BH} = GM_{\rm BH}/v_c^2(R_{\rm BH})$ with $v_c(r)$ given by eq. (10), and we retain the BH only when $v_{\rm kick} < v_c(R_{\rm BH})$. For $M_{\rm BH}/M_{\rm h} = 10^{-3}$, the retention velocity is $v_c(R_{\rm BH}) \sim 2v_{\rm vir}$, where $v_{\rm vir}$ is the escape velocity at the virial radius (Yoo & Miralda-Escudé 2004).

2.3.4 *BH feedback*

There is now strong observational evidence that the energy released by the quasar can drive powerful galaxy-scale outflows (for recent works see Feruglio et al. 2015; Carniani et al. 2015; Cresci et al. 2015 and references therein). Outflowing gas at velocities up to $v \sim 1400$ km/s traced by [CII] emission has been detected in SDSS J1148 (Maiolino et al. 2012) with an estimated total mass outflow rate of $1400 \pm 300\, M_\odot$/yr that decreases with distance from the quasar, ranging from a peak value of $\sim 500\, M_\odot$/yr at ~ 3 kpc to $\lesssim 100\, M_\odot$/yr at ~ 20 kpc (Cicone et al. 2015).

In Valiante et al. (2012) we show that the quasar-driven mass outflow rate predicted by GAMETE/QSOdust, on the basis of a simple energy-driven wind, is in good agreement with the observations. Here we follow a similar approach, adopting the so-called blast wave model, in which the AGN radiation field can accelerate the gas generating fast supersonic winds which propagates outwards through an expanding blast wave, pushing out the surrounding medium (see e.g. Cavaliere et al. 2002; King 2003, 2005, 2010; Lapi et al. 2005; Menci et al. 2005, 2008; Zubovas & King 2012, 2014; Costa et al. 2014 and references therein).

In this framework, the energy released by the AGN that couples with the interstellar gas is estimated as,

$$\dot{E}_{\rm AGN} = \epsilon_{\rm AGN}\, \epsilon_r\, \dot{M}_{\rm accr} c^2, \tag{29}$$

where the coupling efficiency $\epsilon_{\rm AGN}$ is an adjustable free parameter. In our reference model $\epsilon_{\rm AGN} = 1.5 \times 10^{-3}$ (see Table 2).

If the post shock material does not cool efficiently, the bubble expands adiabatically and the outflow is energy-driven. As the blast wave propagates from the center of the halo, it first interacts with the gas of the disk and bulge, reheating a fraction of cold gas and transferring mass to the diffuse hot phase.

When the shock has propagated beyond the bulge and disk radius, part of the gas mass is ejected from the galaxy, if the binding energy is not enough to hold the material.

The mass outflow rate at a given radius r can be estimated as:

$$\dot{M}_{\rm w,AGN}(r) = 2\, \epsilon_{\rm AGN}\, \epsilon_r \left(\frac{c}{v_c(r)}\right)^2 \dot{M}_{\rm accr}, \tag{30}$$

where v_c is the circular velocity of the system given by eq. (10), and we evaluate the above equation at the bulge, disk and DM halo virial radius.

A similar description is used to describe the effects of SN-driven winds. The mass outflow rate beyond a given radius r is given by:

$$\dot{M}_{\rm w,SN}(r) = \frac{2\, \epsilon_{\rm SN}\, E_{\rm SN}}{v_c(r)^2}\, R_{\rm SN} \tag{31}$$

where $R_{\rm SN}$ is the rate of SN explosions, $E_{\rm SN}$ is the average SN explosion energy, and $\epsilon_{\rm SN} = 1.6 \times 10^{-3}$ is the SN wind efficiency (Valiante et al. 2012). The time-dependent SN rate and explosion energy is computed for each galaxy along the merger tree according to formation rate, age and initial mass function of its stellar population. A detailed description of the chemical evolution model can be found in Valiante et al. (2011, 2014) and de Bennassuti et al. (2014).

3 RESULTS

In this section, we present the predicted evolution of the hierarchical assembly of the SMBH and its host galaxy. To explore the dependence of the results on the population of progenitors and their merger rate, for the same model parameters we have run 30 independent merger trees. In one merger tree we find that a merger occurs at $z = 6.43$ between two black holes of $M_{1,\rm BH} = 1.7 \times 10^9 M_\odot$ and $M_{2,\rm BH} = 1.6 \times 10^9 M_\odot$, producing a recoil velocity ~ 2 times higher than the retention speed, $v_c(R_{\rm BH})$. The newly formed BH is displaced from the center and it stops accreting gas. For this reason, we do not consider this to be a viable formation route for a bright quasar like J1148, and we exclude this merger tree from the sample average.

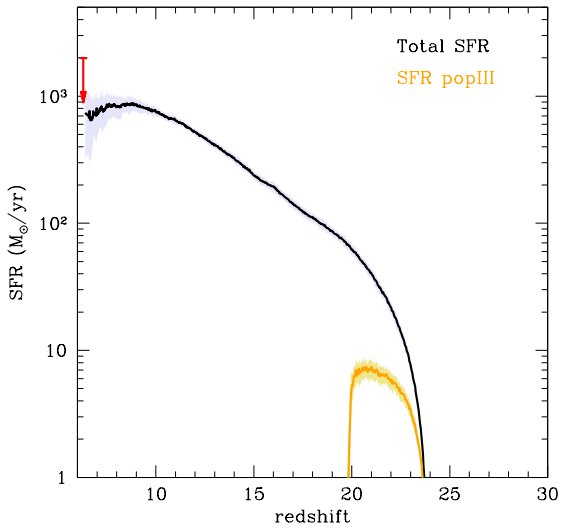

Figure 1. Redshift evolution of the total SFR (black line) and of Pop III stars (orange line), averaged over the 29 realizations. Shaded areas represent 1-σ dispersions and the red arrow indicates the upper limit on the SFR inferred from the IR luminosity (see in the text for further details).

3.1 The formation of stars and BH seeds

In Fig. 1, we show the redshift evolution of the total SFR (summed over all the progenitor galaxies in each simulation) and the separate contribution of Pop III stars. We also show the upper limit on the SFR of $\sim 2000\, M_\odot$/yr (Table 1) inferred from the observed FIR luminosity using the relation $L_{\rm FIR}/L_\odot = 10.84 \times 10^9$ SFR$/(M_\odot/{\rm yr})$ (Valiante et al. 2014). This relation[4] is based on the assumption of starburst dominated dust heating and it provides only an upper limit to the real SFR, due to the non-negligible contribution from the AGN. According to a recent detailed radiative transfer analysis, the AGN can provide up to 60% of the total FIR luminosity (Schneider et al. 2015), decreasing the SFR by a factor 1.4 - 2.5, in agreement with the average value of $\sim 800\, M_\odot$/yr predicted by the reference model.

Due to efficient metal enrichment, Pop III star formation becomes negligible below $z \sim 20$ and no more BH seeds are formed, consistent with other studies (Madau & Rees 2001; Haiman & Loeb 2001; Heger et al. 2003; Volonteri et al. 2003;

[4] The conversion factor between the FIR luminosity and the SFR has been obtained assuming a 10 - 200 Myr burst of stars with solar metallicity and a Larson IMF with $m_{\rm ch} = 0.35 M_\odot$ (Valiante et al. 2014).

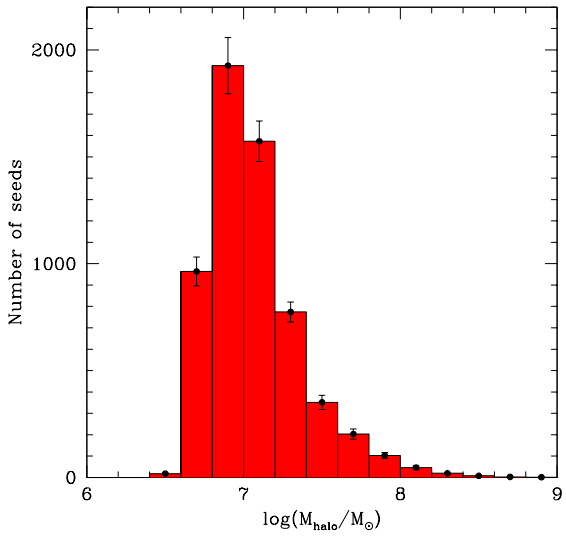

Figure 2. Mass distribution of halos hosting a newly formed 100 $M_\odot$ BH seed, averaged over the 29 realizations with 1-σ error bars.

Madau et al. 2004; Valiante et al. 2016. The mass distribution of DM halos which host BH seeds ranges between $\sim 3\times10^6 M_\odot$ and $\sim 10^8 M_\odot$ with a peak at $M_h \sim 10^7 M_\odot$, as shown in Fig. 2. Thus, we find that a major fraction ($\sim$ 90%, on average) of BH seeds are formed in DM mini-halos, where gas cooling could be easily suppressed due to H_2 photo-dissociation by Lyman-Werner photons. The inclusion of this additional feedback effect slows down metal enrichment and extends BH seeds formation to lower redshifts ($z \geq 15$) and larger DM halos ($\sim 5\times10^7 - 10^9 M_\odot$). While the evolution of the total BH mass and BH accretion rate at $z < 15$ is only mildly affected, the birth environment of late-forming seed BHs (gas rich Ly-α cooling halos) may be more favorable to SE accretion. Here we do not consider the effect of H_2 photo-dissociation, which we defer to a future study, and we assume that the formation rate of Pop III stars is limited only by metal enrichment.

3.2 BH evolution

In Fig. 3 we show the redshift evolution of the BH mass and black hole accretion rate (BHAR) predicted by our reference model. In the top panels, the values are obtained summing over all BH progenitors present at each redshift in each simulation and then averaged over the 29 realizations. The different lines allow to separate the contribution to the BH mass and accretion rate achieved by means of sub-Eddington ($\leq 16\, L_{\rm Edd}/c^2$) and super-Eddington ($> 16\, L_{\rm Edd}/c^2$) accretion events. By construction, the final BH mass predicted by the reference model is $\sim (3.6 \pm 1.6)\times10^9 M_\odot$, in agreement with the value inferred from observations of J1148 (see Table 1). We find that, on average, $\sim$ 75% of the final SMBH mass grows by means of super-Eddington gas accretion. This provides the dominant contribution to the total BHAR at all but the smallest redshifts. Although the quantities shown in all panels have been averaged over 29 merger trees, the redshift evolution of the BHAR appears to be very intermittent, a consequence of rapid depletion/replenishment of the bulge gas reservoir out of which the BHs accrete.

To gain a better idea of the typical values of BH mass and BHAR predicted by the reference model, in the bottom panels of Fig. 3 we also show the mean quantities, averaged over all BH progenitors present at each redshift in each simulation. It is clear that at $20 \lesssim z \lesssim 25$ the mean BH mass rapidly grows from $\sim 100\, M_\odot$ to $\sim 10^4\, M_\odot$ by means of super-Eddington gas accretion rates of $10^{-5} M_\odot/{\rm yr} \lesssim {\rm BHAR} \lesssim 10^{-3} M_\odot/{\rm yr}$. Hence, due to early efficient super-Eddington accretion, the mean BH progenitors at $z \sim 20$ have already achieved a mass comparable to the BH mass predicted by the direct collapse scenario. This is consistent with what recently found by Lupi et al. (2015) by means of high-resolution numerical simulations, which show that stellar-mass black holes can increase their mass by 3 orders of magnitudes within a few million years while accreting gas at super-Eddington rates in the dense cores of high-z galaxies.

Fig. 4 shows the average distribution of BHs accreting at super- and sub-Eddington rates as a function of the BH mass and Eddington accretion ratio for different redshift intervals. The reference model predicts that, at $15 \leq z \leq 25$, almost all BH progenitors accrete at super-Eddington rates. Since the BH masses are still relatively small, $10^2\, M_\odot \leq M_{\rm BH} \leq 10^6\, M_\odot$, BH accretion rates of $10^{-5} M_\odot/{\rm yr} \lesssim {\rm BHAR} \lesssim 5\times10^{-3} M_\odot/{\rm yr}$, which characterize the early mass growth (see the bottom right panel of Fig. 3), correspond to very large accretion ratios, $\dot{M}_{\rm accr}/\dot{M}_{\rm Edd} \sim 10^2 - 10^4$. The mass of BH progenitors increases with time and the fractional number of super-Eddington accreting BHs decreases, being $f_s \sim 60\%$ at $z \sim 10-15$ and dropping to $f_s \sim 20\%$ at $z < 10$. Because of the larger BH masses, the accretion ratios are smaller and $\dot{M}_{\rm accr}/\dot{M}_{\rm Edd} < 500$ at $z < 10$.

For most of the evolution, we find that BH progenitors accrete at highly super-Eddington rates, with $\dot{M}_{\rm accr}/\dot{M}_{\rm Edd} >> 10$. At these large Eddington accretion ratios the applicability of the adopted slim disk solution is highly debated. In fact, recent general-relativistic magneto-hydrodynamical simulations show that BHs accreting at $20 < \dot{M}_{\rm accr}/\dot{M}_{\rm Edd} < 200$ develop a disk structure that is still radiatively inefficient, with total luminosities that do not exceed $\sim 10\, L_{\rm Edd}$, but the total energy escaping the system can be very large, mostly in the form of thermal and kinetic energy of outflowing gas and Poyinting flux (McKinney et al. 2014; Sądowski et al. 2013). However, Inayoshi et al. (2015) have shown that there exist regimes where steady accretion rates larger than 3000 times the Eddington rate can be sustained.

To better assess the impact of these extreme hyper-Eddington accretion events on our results, we have run the same set of simulations discussed so far but artificially imposing an upper limit of $\dot{M}_{\rm accr} \leq 20\, \dot{M}_{\rm Edd} = 320\, L_{\rm Edd}/c^2$ to the gas accretion rate. The results are shown in Fig. 5. In the same figure, we also show, for comparison, the evolution predicted assuming Eddington-limited accretion. In order to better compare with previous results, this model has been run assuming $\dot{M}_{\rm accr} \leq L_{\rm Edd}/c^2$ (1/16 smaller than the definition adopted in the present study, see Eq. 25), as conventionally adopted in the literature.

We find that, even when the Eddington accretion ratio is $\dot{M}_{\rm accr}/\dot{M}_{\rm Edd} \leq 20$, the final SMBH mass predicted by the reference model is in good agreement with the observations. The high-redshift evolution of both the total BH mass and the total BHAR, however, is markedly different from the results shown in Fig. 3. At $z > 10$ the BHAR is several orders of magnitudes smaller and the BH mass is correspondingly affected, being $\sim 10^6\, M_\odot$ at $z \sim 15$ ($\sim 1/100$ of the total BH mass shown in Fig. 3 at the same z). Due to the smaller gas accretion rates at high redshifts, a larger gas fraction is retained around nuclear BHs at $z < 10$. As a result, the BH

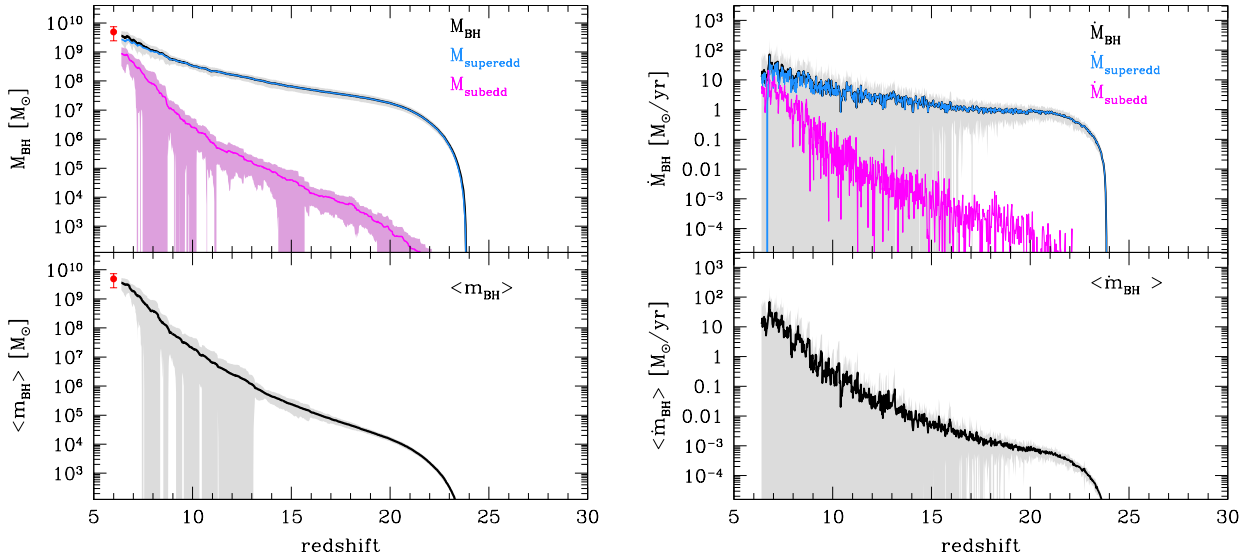

Figure 3. Redshift evolution of the total and mean BH masses and BHARs, averaged over 29 independent merger trees. Shaded areas are 1-σ dispersions. *Top, left panel*: total BH mass (summed over all BH progenitors at each redshift in each simulation, black line) and the BH mass grown by means of sub-Eddington (magenta line) and super-Eddington (cyan line) accretion events. *Top, right panel*: total BHAR (black line) and BHAR obtained considering only sub- (magenta line) and super- (cyan line) Eddington accreting BHs. The mean BH mass and BHAR (averaged over all BH progenitors at each redshift in each simulation) are shown in the bottom panels (left and right, respectively).

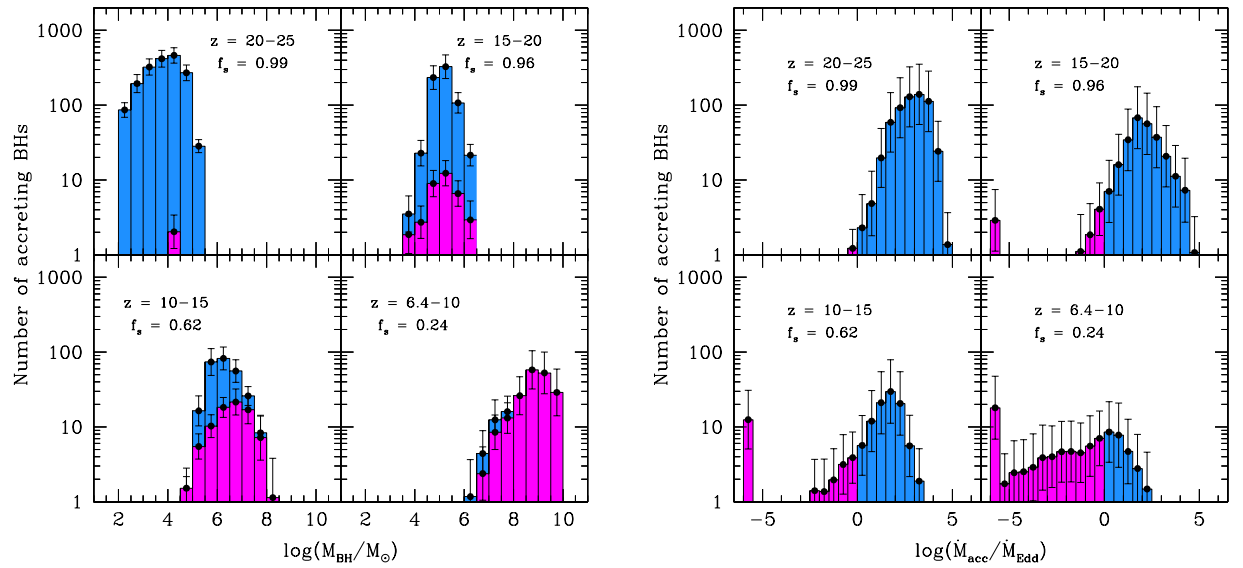

Figure 4. Number of accreting BHs as a function of the black hole mass (*left panel*) and the accretion ratio (*right panel*), averaged over 29 realizations with 1−σ error bars. The histograms show the number of super- (cyan) and sub- (magenta) Eddington accreting BHs. In each figure, we separately show 4 different redshift intervals and we give the corresponding number fraction of super-Eddington accreting BHs over the total, f_s.

mass has a steeper late growth rate, with short episodes of intense gas accretion reaching $\sim 10^2\ M_\odot$/yr at $z \sim 7$.

On the contrary, when Eddington-limited gas accretion is assumed, the final BH mass can no longer be reproduced using the reference model. In this case, the gas accretion rates are too small to trigger fast BH growth at high redshifts. The total BH mass is dominated by the coalescence of BH seeds and its redshift evolution is strongly affected by lack of BH seeds at $z < 20$ (see the behaviour of the Pop III SFR in Fig. 1) and by kicks received during BH-BH coalescences in major mergers. Fig. 6 shows the evolution of the average number of major mergers and of kicked BHs predicted by the model. While the average number of major mergers decreases

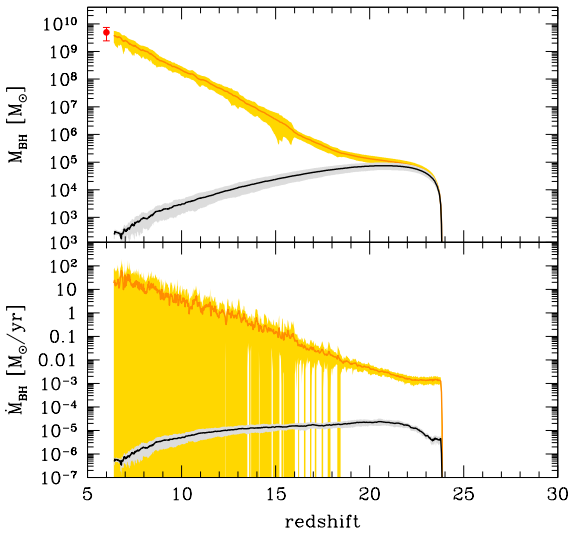

Figure 5. Redshift evolution of the total BH mass (*upper panel*) and BHAR (*lower panel*), averaged over 29 independent merger trees. Shaded areas are 1-σ dispersions. In each panel, the orange line indicates the predicted evolution assuming $\dot{M}_{\rm accr} \leq 20\,\dot{M}_{\rm Edd} = 320\,L_{\rm Edd}/c^2$ and the black line shows the evolution assuming the conventional Eddington limited accretion, $\dot{M}_{\rm accr} \leq L_{\rm Edd}/c^2$ (see text).

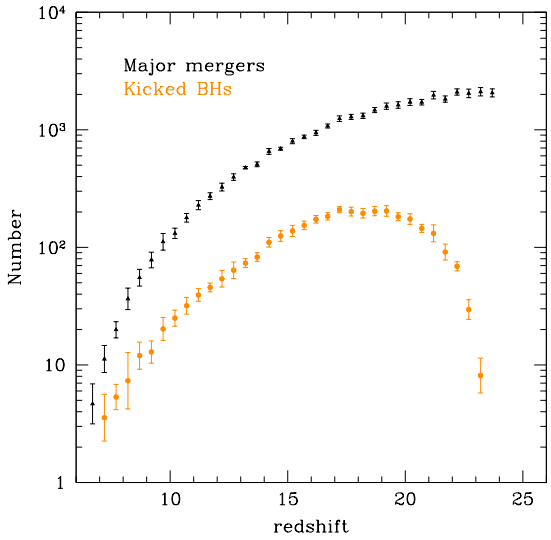

Figure 6. The average redshift distribution of major mergers (black triangles) and of kicked BHs during BH-BH coalescences in the model where $\dot{M}_{\rm accr} \leq L_{\rm Edd}/c^2$ (orange points). Each point has been obtained averaging over 29 different merger tree realizations and the errorbars correspond to the 1-σ dispersion.

with time, the number of kicked BHs increases at $20 \lesssim z \lesssim 25$ and than decreases at lower z. This is due to the combination of the growing number of BH seeds formed at high z and of the shallow potetial wells of their host mini-halos, which allow the kick velocity of the newly formed BH to easily exceed the retention speed.

Hence, we can conclude that super-Eddington accretion is fundamental for the formation of the first SMBHs at $z > 6$, even when extreme hyper-Eddington accretion events are not considered.

3.3 Environmental conditions for Super-Eddington accretion

Our model enables us to perform a statistical study of the physical properties of the environments where BH progenitors accrete at super-Eddington rates. The left panel of Fig. 4 shows that when both sub- and super-Eddington accreting BHs are present, their BH masses are comparable, with a tendency of sub-Eddington accreting BHs to have larger masses at lower z. Similarly, the occurrence of super-Eddington accretion is not correlated with the mass of the host dark matter halo, nor with its gas content or metallicity. At each given value of any of these quantities, in fact, both sub- and super-Eddington accreting BHs are found in the simulations.

The different accretion regimes are more cleanly separated when we plot the Eddington gas accretion ratio as a function of the ratio between the gaseous bulge and the BH masses (see the left panel of Fig. 7). Most of the BHs that accrete at sub-Eddington rates are characterized by $M_{\rm b}/M_{\rm BH} < 20$, whereas the number of super-Eddington accreting BHs is negligible when $M_{\rm b}/M_{\rm BH} < 0.1$. However, when $0.1 \leq M_{\rm b}/M_{\rm BH} \leq 20$ (the region between the two vertical lines in the plot), the BHs can be characterized by vastly different accretion ratios: a good fraction of the hyper-Eddington accreting BHs are found in this region of the plot. The larger accretion rate in these systems is due to the much shorter dynamical time of the bulge. This is shown in the right panel of Fig. 7. A sequence of increasing bulge dynamical times is evident, with most of the BHs found in bulges with $0.01\,{\rm Myr} \lesssim \tau_{\rm b} < 1\,{\rm Myr}$ in hyper-Eddington, $0.1\,{\rm Myr} \lesssim \tau_{\rm b} < 20\,{\rm Myr}$ in mildly super-Eddington, and $5\,{\rm Myr} \lesssim \tau_{\rm b} < 20\,{\rm Myr}$ in sub-Eddington accretion regimes. Indeed, hyper-Eddington accreting BHs are predominantly found in high-z systems, with less massive and more compact bulges. The figure also shows that super-Eddington accretion requires gas-rich bulges and that, when $M_{\rm b}/M_{\rm BH} < 0.1$, only sub-Eddington accreting BHs in massive, gas poor bulges are found.

The environmental conditions for super-Eddington accretion that emerge from our statistical study are in good agreement with the results recently found by Lupi et al. (2015). By means of detailed hydro-dynamical simulations, these authors show that, in order to accrete at super-Eddington rates, BHs must be embedded in dense gas structures, with masses comparable or larger than the masses of the accreting BHs.

3.4 BH-driven outflow

Outflowing cold gas in J1148, traced by [C II] emission, was first detected by Maiolino et al. (2012) with the IRAM Plateau de Bure Interferometer, and then confirmed with high-resolution follow-up observations by Cicone et al. (2015). The outflow has a complex morphology and spatial extent, reaching a maximum projected radius of 30 kpc. The estimated mass outflow rate and velocity are shown in Fig. 8 as a function of the projected distance from the nucleus. In the same figure, we also show the predictions of the reference model. Following eq. (30), the outflow velocity is computed as the circular velocity at the corresponding radius, $v_{\rm w,AGN}(r) = v_{\rm c}(r)$, and we estimate the mass outflow rate accounting for the delay $\tau_{\rm dyn} = r/v_{\rm w,AGN}$ between the BH energy release and the observation. Due to the large variability of the BH luminosity, the 1-σ dispersion among the different merger trees of the predicted average mass outflow rate (gray shaded region in the upper panel) is con-

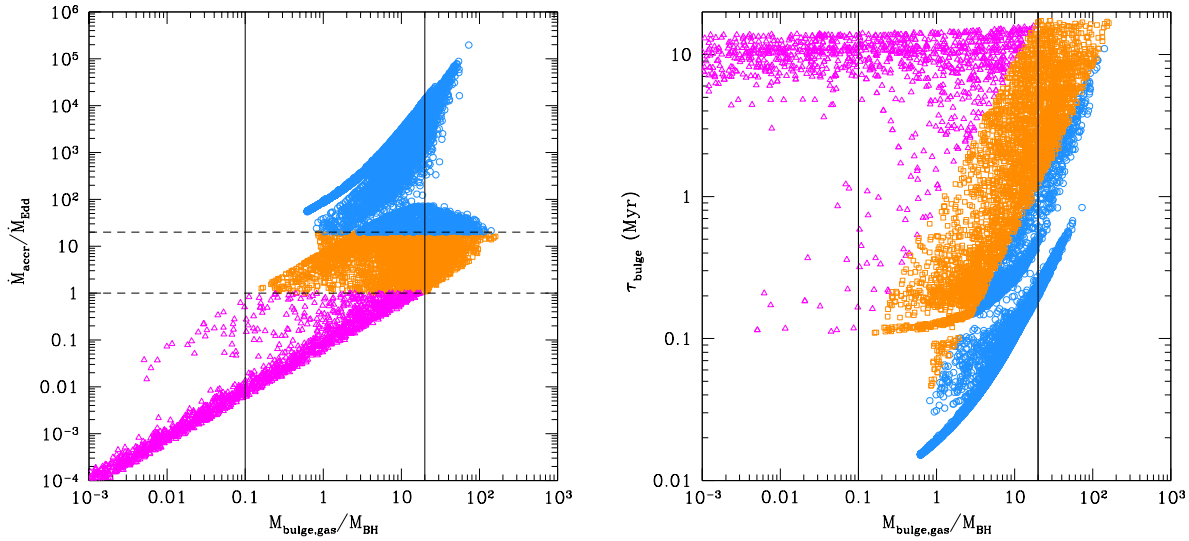

Figure 7. Eddington accretion ratio, $\dot{M}_{\rm accr}/\dot{M}_{\rm Edd}$, (*left panel*) and dynamical timescale of the bulge, $\tau_{\rm b}$, (*right panel*) as a function of the bulge gas - BH mass ratio, $M_{\rm b}/M_{\rm BH}$. Each point represents an accreting BH in any of the 29 merger histories. Sub-Eddington accreting BHs are shown by magenta triangles, and we separate mildly super-Eddington accreting BHs with $1 \leq \dot{M}_{\rm accr}/\dot{M}_{\rm Edd} \leq 20$ (orange squares) and hyper-Eddington accreting BHs with $\dot{M}_{\rm accr}/\dot{M}_{\rm Edd} > 20$ (cyan circles). The two horizontal dashed lines in the left panel allow to visually separate these regimes. The vertical lines in both panels give two reference values of $M_{\rm b}/M_{\rm BH} = 0.1$ and 20 (see text).

sistent with the data. However, the average values (black solid line) are larger than observed and show a different radial dependence, especially at $r > 20$ kpc. The bottom panel shows that the observed outflow travels at a velocity consistent with the circular velocity of the host system. There are a few radii where the observed values are larger, probably reflecting a stronger coupling between the energy and momentum injected by the AGN and the surrounding gas. Yet, even if we take the observed values of outflow velocities at each radius to estimate $\tau_{\rm dyn}$ and $\dot{M}_{\rm w,AGN}$ (see the blue dashed line in the upper panel with the cyan shaded region), the resulting mean mass outflow rate is still larger than observed. Our description of an energy-driven wind with constant coupling efficiency may not be adequate to capture the complex dynamics of this massive outflow. However, Cicone et al. (2015) stress that the data should be considered as a lower limit on the total mass outflow rate, because it accounts only for the atomic gas phase of the outflow, while a significant amount of the outflowing mass may be in the molecular phase.

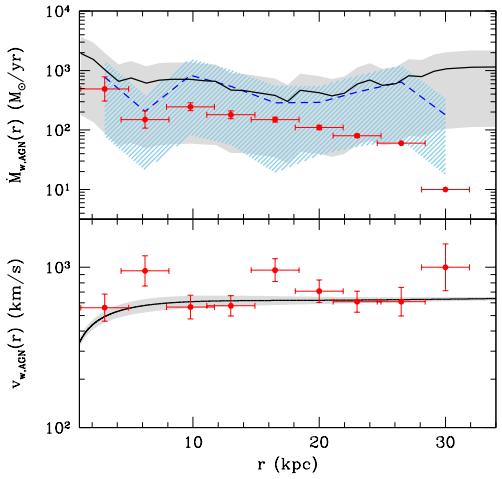

Figure 8. The mass outflow rate (*upper panel*) and velocity (*lower panel*) as a function of the projected distance from the nucleus. Cicone et al. (2015) observations are shown with red data points and the predictions of the reference model are shown by black solid lines with shaded gray regions. The blue dashed line in the upper panel (with the cyan dashed region) shows the predicted outflow rate that we would infer using the BH luminosity predicted by the reference model and the observed outflow velocities (see text). The lines show the average among the 29 merger trees and the shaded regions are the 1-σ dispersion.

3.5 The coevolution of BHs and their host galaxies

It is interesting to explore the implications of our results for the co-evolution of nuclear BHs and their host galaxies. In Fig. 9 we show the evolutionary path (from the bottom left to the top right) in the mean BH mass - stellar bulge mass ($\langle m_{\rm BH}\rangle$ - $\langle m_{\rm b}^{\star}\rangle$) plane predicted by the reference model (black solid line) and by the model with $\dot{M}_{\rm accr} \leq 20\,\dot{M}_{\rm Edd}$ (orange solid line). In each simulation, we consider the mean values among all the SMBH progenitors and their hosts present at each redshift, and then we average over the 29 merger trees. For comparison, we also show in the same figure the observational data and the empirical fit (gray data points and dashed line) for local galaxies provided by Sani et al. (2011), and the more recent scaling relation inferred for local ellipticals and classical bulges by Kormendy & Ho (2013, solid green line and shaded region).

In the reference model, BH progenitors of the first SMBHs at $z > 6$ follow a symbiotic evolution, with a small offset with respect to the observed local scaling relation. When $\dot{M}_{\rm accr} \leq 20\,\dot{M}_{\rm Edd}$,

the different evolution at high-z is reflected in a steeper relation between the mean BH mass and the stellar bulge, very close to that predicted by Kormendy & Ho (2013). The difference between the models becomes negligible when $\langle m_{\rm BH}\rangle > 10^7\,M_\odot$ ($\langle m_{\rm b}^\star\rangle > 10^9\,M_\odot$), which occurs - on average - at $z \sim 10$.

When the average BH mass has reached its value of $(3.6 \pm 1.6) \times 10^9 M_\odot$ at $z = 6.4$, the host galaxy has already grown to a bulge (total) stellar mass of $2.7\,(3.2) \times 10^{11}\,M_\odot$. Hence, we predict a final average BH-to-bulge (total) stellar mass ratio of $M_{\rm BH}/M_{\rm star} = 0.013\,(0.011)$, well within the scatter of the relations inferred from various observational studies of massive local galaxies (Marconi & Hunt 2003; Sani et al. 2011; Kormendy & Ho 2013, and references therein). However, this ratio is ~ 25 times smaller than what is inferred from observations of J1148 (red data point). Following the procedure commonly applied to high-z bright QSOs, the stellar mass is computed as $M_{\rm star} = M_{\rm dyn} - M_{\rm H_2}$, with $M_{\rm dyn}$ and $M_{\rm H_2}$ inferred from CO observations (see Table 1, Walter et al. 2004; Wang et al. 2010). Similar results obtained for a larger sample of $z > 6$ QSOs have suggested the idea that the first SMBHs grow faster than their host galaxies (Wang et al. 2010, 2013; Venemans et al. 2015 see however Willott et al. 2015).

As suggested by Valiante et al. (2014), observations of high-z QSOs are sensitive to the innermost 2.5 – 3 kpc and may be missing a significant fraction of the galaxy (Valiante et al. 2014). This is also supported by recent observations of J1148, which show extended [C II] 158 μm emission and far-infrared (FIR) continuum, likely associated with cold gas and star formation on scales of $\sim 10 - 20$ kpc (Cicone et al. 2015).

Indeed, the mean bulge effective radius at $z = 6.4$ predicted by the model is $R_{\rm eff} = 7.3 \pm 0.8$ kpc, in good agreement with observations of local galaxies hosting the largest BHs (see Fig. 10). When we restrict to the innermost 2.5 kpc, we find a mean bulge stellar mass of $(3.9 \pm 0.2) \times 10^{10}\,M_\odot$, much closer to the observation (see the arrow and black data point in Fig. 9). The same is true if we consider the mean gas mass within 2.5 kpc, that we predict to be $M_{\rm H_2} = (2.0 \pm 0.9) \times 10^{10}\,M_\odot$, that well reproduce the observed value (see Table 1).

Finally, the reference model predicts a mean dust mass at $z = 6.4$ of $M_{\rm dust} = (3.6 \pm 0.9) \times 10^8\,M_\odot$, in good agreement with the value inferred from the FIR luminosity. This result has been obtained using the chemical evolution module, which includes dust processing in a 2-phase ISM, that has been developed by Valiante et al. (2011, 2014) and de Bennassuti et al. (2014). Hence, consistent with previous findings (Valiante et al. 2011, 2014), we find that the large dust mass that has enriched the ISM of the host galaxy is the result of a large stellar component, and that the apparent tension with the observed dynamical mass - the so-called *stellar mass crisis* - is at least partly due to the small spatial extent of the observations. We refer the interested readers to Valiante et al. (2014) for an extended discussion on this point.

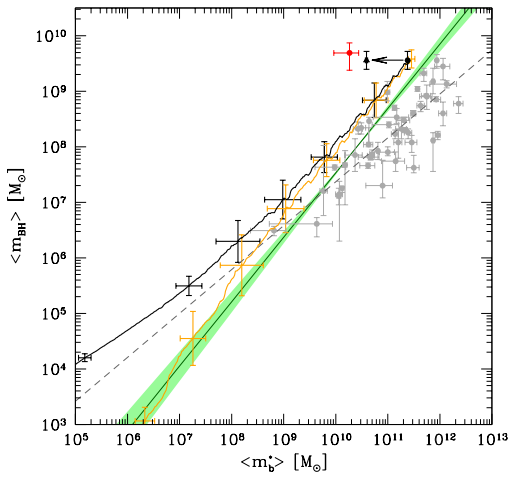

Figure 9. Redshift evolution of the mean black hole mass as a function of the mean bulge stellar mass in SMBH progenitors for the reference model (black solid line) and the model with $\dot{M}_{\rm accr} \leq 20\,\dot{M}_{\rm Edd}$ (orange solid line). Gray circles are data for local galaxies, with the empirical fit (gray dashed line) provided by Sani et al. (2011). The solid green line with shaded region is the scaling relation derived by Kormendy & Ho (2013). The red point represents the black hole and stellar mass within a region of 2.5 kpc inferred from observations of J1148 (Table 1). The model predictions are averaged over 29 merger tree realizations and the errorbars show the 1-σ dispersion for both mean BH and bulge stellar mass, at few selected redshift along the averaged merger histories. The arrow illustrates the reduction in stellar mass if we restrict to the central 2.5 kpc region (black data point, see text).

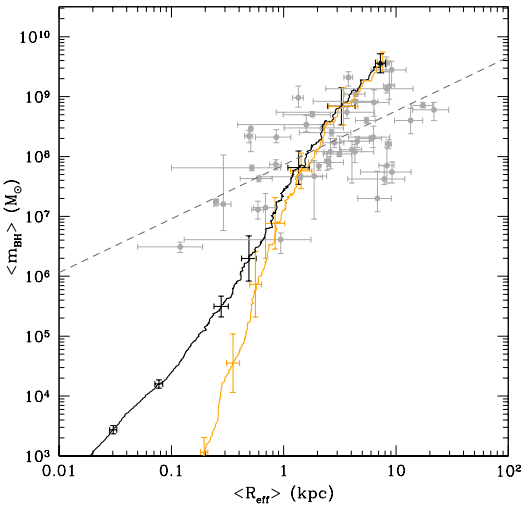

Figure 10. Redshift evolution of the mean black hole mass as a function of the mean bulge effective radius of the host galaxy, averaged over 29 merger tree realizations with 1-σ errorbars at few selected redshift, for the reference model (black solid line), and the model with $\dot{M}_{\rm accr} \leq 20\,\dot{M}_{\rm Edd}$ (orange solid line). Gray circles represent data for local galaxies, with the empirical fit (gray dashed line) given by Sani et al. (2011).

4 DISCUSSION AND CONCLUSIONS

The data-constrained model GAMETE/QSOdust allows us to explore a large number of formation histories of a given quasar, in the present case J1148 at $z = 6.4$, reproducing the observations of the quasar and its host galaxy. With the adjustable free parameters that we have selected, described in Table 2, the model reproduces the physical quantities listed in Table 1. Hence, the properties that we predict for the host galaxy of J1148 (SFR, dust mass, gas

and stellar masses) are consistent with previous results obtained by (Valiante et al. 2014, 2016) for the same quasar.

With respect to (Valiante et al. 2011, 2014, 2016), the current version of GAMETE/QSOdust enables to (*i*) follow the formation and evolution of the disk and bulge in each progenitor galaxy, and (*ii*) remove the constraint of Eddington-limited BH accretion.

In particular, Valiante et al. (2016) find that the formation of a few (between 3 and 30 in the reference model) heavy BH seeds with masses $M_{\rm BH} = 10^5\,M_\odot$ enables the Eddington-limited growth of a SMBH by $z = 6.4$. This conclusion heavily depends on the occurrence - among the progenitors - of Lyman-α cooling halos where gas cooling is suppressed by the low-metallicity and strong Lyman-Werner background (Valiante et al. 2016). This "head start" requires favourable conditions, that are easily erased by the joint interplay of chemical, radiative and mechanical feedback effects.

Here we have explored the alternative scenario where the BHs can grow through a radiatively inefficient slim disk at super-Eddington rates. This condition is easily met by light BH seeds formed in gas-rich systems at high redshifts.

In the model presented in this work, we plant light BH seeds in newly virialized halos above redshift $z \sim 20$, before the effects of chemical feedback inhibit the formation of metal poor ($Z < Z_{\rm cr}$) stars. With this seeding prescription, we find that:

- On average, $\sim 80\%$ of the SMBH mass of J1148 is provided by super-Eddington gas accretion ($> 16\,L_{\rm Edd}/c^2$). This represents the dominant contribution to BH growth down to $z \sim 10$;
- Due to fast and efficient super-critical accretion, the mean BH mass at redshift $z \sim 20$ is $\gtrsim 10^4\,M_\odot$, comparable that predicted for heavy BH seeds formed by direct collapse;
- More than 90% of BH progenitors accrete at super-Eddington rates at $15 < z < 25$ in dense, gas-rich environments. At these redshifts, hyper-Eddington accretion events, with $\dot{M}_{\rm accr}/\dot{M}_{\rm Edd} \sim 10^2 - 10^4$, are common;
- The observed SMBH mass of J1148 at $z = 6.4$ can be reproduced even adopting a maximum super-Eddington accretion rate of $\dot{M}_{\rm accr} \leq 20\,\dot{M}_{\rm Edd}$, showing that hyper-critical accretion is not required;
- BH progenitors of the final SMBH evolve in symbiosis with their host galaxies. The predicted AGN-driven mass outflow rate at $z = 6.4$ shows a radial profile that is broadly consistent with the lower limits inferred from CII observations by Cicone et al. (2015);
- The predicted final BH-to-bulge (total) stellar mass ratio, $M_{\rm BH}/M_{\rm star} = 0.013\,(0.011)$, is within the scatter of the observed local relation and a factor of ~ 25 lower than inferred from dynamical mass observations of J1148. The discrepancy is significantly reduced if we account for the mass within 2.5 kpc from the nucleus, the region targeted by CO data. At this radius, the mean bulge stellar mass is $(3.9 \pm 0.2) \times 10^{10}\,M_\odot$, much closer to the observational value.

As a consequence of the lower gas accretion rates, the average BH mass predicted by Valiante et al. (2016) is much smaller than in our reference model, at all but the latest redshifts (see their Fig. 3). This difference is reduced when we impose that $\dot{M}_{\rm accr} \leq 20\,\dot{M}_{\rm Edd}$. In this case, the average BH progenitor mass at $z \sim 15$ is comparable in the two models. However, while in Valiante et al. (2016) the mass growth is triggered by the formation of heavy seeds, in our model this is achieved by mildly super-Eddington accretion on light BH seeds.

The progenitors of SMBHs at $z > 6$ experience the *strong* form of coevolution defined by Kormendy & Ho (2013), where galaxies affect BH growth by controlling BH feeding and merging,

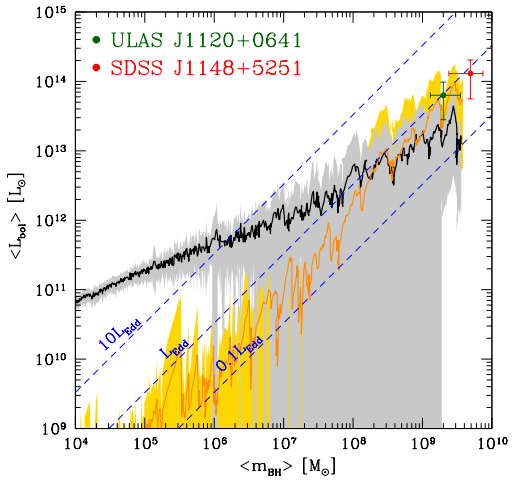

Figure 11. Mean bolometric luminosity of BH progenitors as a function of the mean BH mass predicted by the reference model (black solid line) and by the model with $\dot{M}_{\rm accr} \leq 20\,\dot{M}_{\rm Edd}$ (yellow solid line). For each model, the lines show the average among the 29 merger trees and the shaded regions are the 1-σ dispersion. The data points show the observational values of the two quasars SDSS J1149 (red circle) and ULAS J1120 (green square). The diagonal dashed lines show some reference values of the luminosity in units of the Eddington luminosity.

and BHs control galaxy properties via AGN feedback. In fact, while the small radiative efficiencies of super-Eddington accreting BHs is indispensable to limit the effects of AGN feedback (Lupi et al. 2015), at $z > 10$ the BHs shine at a few Eddington luminosities with a noticeable effect on the cold gas content of their host galaxies. At lower z, an increasing fraction of BH progenitors accrete at sub-Eddington rates, but with larger radiative efficiencies. As a result of the larger BH mass and BH accretion rates, AGN-driven winds at $z < 10$ power strong galaxy-scale outflows and suppress star formation, leading to the down-turn of the total SFR shown in Fig. 1.

In Fig. 11 we show the average bolometric luminosity as a function of the average BH mass of SMBH progenitors for the reference model (black solid line) and for the model with $\dot{M}_{\rm accr} \leq 20\,\dot{M}_{\rm Edd}$ (yellow solid line). The model predictions are compared with observations of SDSS J1148 ($z = 6.4$) and of the most distant quasar currently known, ULAS J1120 at $z = 7.1$ (Mortlock et al. 2011). The errorbars on the bolometric luminosities account for the observational uncertainties on the flux at 1450 Å and on the bolometric corrections (Richards et al. 2006). Some reference values of the luminosity in units of the Eddington luminosity are shown by the diagonal dashed lines. The difference among the two models reflects the different BH accretion history: in the model with $\dot{M}_{\rm accr} \leq 20\,\dot{M}_{\rm Edd}$ the first BH progenitors accrete at a lower rate, saving cold gas for the latest evolutionary phases. As a result, for BH progenitors with $M_{\rm BH} \lesssim 10^8\,M_\odot$, the mean luminosity predicted by the reference model is always super-Eddington (with $L_{\rm bol} > 10\,L_{\rm Edd}$ when $M_{\rm BH} \lesssim 10^6\,M_\odot$), whereas in the model with $\dot{M}_{\rm accr} \leq 20\,\dot{M}_{\rm Edd}$ the mean luminosity is always $0.1\,L_{\rm Edd} < L_{\rm bol} < L_{\rm Edd}$. However, in the latest evolutionary phases, when $M_{\rm BH} > 10^8\,M_\odot$, this trend is reversed. Given the observational uncertainties and the large variability among different merger trees, the luminosity of J1148 is consistent with the model predictions. Interestingly, the data point of ULAS J1120 is also lying within the 1-σ dispersion. Indeed, we

find that ∼ 20% of BH progenitors at $z = 7.1$ have luminosities and masses compatible with the observed values of ULAS J1120, indicating that this quasar may be one of the progenitors of SDSS J1148 at $z = 6.4$.

ACKNOWLEDGMENTS

We thank Valeria Ferrari, Nicola Menci and Marta Volonteri for useful discussions and comments. The research leading to these results has received funding from the European Research Council under the European Unions Seventh Framework Programme (FP/2007-2013) / ERC Grant Agreement n. 306476.

REFERENCES

Abel T., Bryan G. L., Norman M. L., 2002, Science, 295, 93
Abramowicz M. A., Czerny B., Lasota J. P., Szuszkiewicz E., 1988, ApJ, 332, 646
Baker J. G., Boggs W. D., Centrella J., Kelly B. J., McWilliams S. T., Miller M. C., van Meter J. R., 2008, ApJ, 682, L29
Barausse E., 2012, MNRAS, 423, 2533
Begelman M. C., Volonteri M., Rees M. J., 2006, MNRAS, 370, 289
Bournaud F., Combes F., Jog C. J., Puerari I., 2005, A&A, 438, 507
Bromm V., Loeb A., 2003, ApJ, 596, 34
Bromm V., Coppi P. S., Larson R. B., 2002, ApJ, 564, 23
Campanelli M., Lousto C., Zlochower Y., Merritt D., 2007, ApJ, 659, L5
Carniani S., et al., 2015, A&A, 580, A102
Cavaliere A., Lapi A., Menci N., 2002, ApJ, 581, L1
Cicone C., et al., 2015, A&A, 574, A14
Costa T., Sijacki D., Haehnelt M. G., 2014, MNRAS, 444, 2355
Cox T. J., Jonsson P., Somerville R. S., Primack J. R., Dekel A., 2008, MNRAS, 384, 386
Cresci G., et al., 2015, ApJ, 799, 82
Davies M. B., Miller M. C., Bellovary J. M., 2011, ApJ, 740, L42
De Lucia G., Boylan-Kolchin M., Benson A. J., Fontanot F., Monaco P., 2010, MNRAS, 406, 1533
De Rosa G., Decarli R., Walter F., Fan X., Jiang L., Kurk J., Pasquali A., Rix H. W., 2011, ApJ, 739, 56
Devecchi B., Volonteri M., 2009, ApJ, 694, 302
Devecchi B., Volonteri M., Colpi M., Haardt F., 2010, MNRAS, 409, 1057
Devecchi B., Volonteri M., Rossi E. M., Colpi M., Portegies Zwart S., 2012, MNRAS, 421, 1465
Fan X., et al., 2001, AJ, 122, 2833
Fan X., et al., 2003, AJ, 125, 1649
Fan X., et al., 2004, AJ, 128, 515
Ferrara A., Salvadori S., Yue B., Schleicher D., 2014, MNRAS, 443, 2410
Feruglio C., et al., 2015, A&A, 583, A99
Greif T. H., Bromm V., Clark P. C., Glover S. C. O., Smith R. J., Klessen R. S., Yoshida N., Springel V., 2012, MNRAS, 424, 399
Haiman Z., 2004, ApJ, 613, 36
Haiman Z., Loeb A., 2001, ApJ, 552, 459
Haiman Z., Rees M. J., Loeb A., 1996, ApJ, 467, 522
Heger A., Fryer C. L., Woosley S. E., Langer N., Hartmann D. H., 2003, ApJ, 591, 288
Hernquist L., 1990, ApJ, 356, 359
Hirano S., Hosokawa T., Yoshida N., Omukai K., Yorke H. W., 2015, MNRAS, 448, 568
Inayoshi K., Haiman Z., Ostriker J. P., 2015, preprint, (arXiv:1511.02116)
Kelly B. C., Shen Y., 2013, ApJ, 764, 45
Khlopov M. Y., Rubin S. G., Sakharov A. S., 2005, Astroparticle Physics, 23, 265
King A., 2003, ApJ, 596, L27
King A., 2005, ApJ, 635, L121
King A. R., 2010, MNRAS, 402, 1516
Kormendy J., Ho L. C., 2013, ARA&A, 51, 511
Koushiappas S. M., Bullock J. S., Dekel A., 2004, MNRAS, 354, 292
Lacey C., Cole S., 1993, MNRAS, 262, 627
Lapi A., Cavaliere A., Menci N., 2005, ApJ, 619, 60
Lodato G., Natarajan P., 2006, MNRAS, 371, 1813
Lupi A., Colpi M., Devecchi B., Galanti G., Volonteri M., 2014, MNRAS, 442, 3616
Lupi A., Haardt F., Dotti M., Fiacconi D., Mayer L., Madau P., 2015, preprint, (arXiv:1512.02651)
Madau P., Rees M. J., 2001, ApJ, 551, L27
Madau P., Rees M. J., Volonteri M., Haardt F., Oh S. P., 2004, ApJ, 604, 484
Madau P., Haardt F., Dotti M., 2014, ApJ, 784, L38
Magorrian J., et al., 1998, AJ, 115, 2285
Maiolino R., et al., 2012, MNRAS, 425, L66
Marconi A., Hunt L. K., 2003, ApJ, 589, L21
McKinney J. C., Tchekhovskoy A., Sadowski A., Narayan R., 2014, MNRAS, 441, 3177
Menci N., Cavaliere A., Fontana A., Giallongo E., Poli F., Vittorini V., 2004, ApJ, 604, 12
Menci N., Fontana A., Giallongo E., Salimbeni S., 2005, ApJ, 632, 49
Menci N., Fiore F., Puccetti S., Cavaliere A., 2008, ApJ, 686, 219
Middleton M. J., et al., 2013, Nature, 493, 187
Mihos J. C., Hernquist L., 1994, ApJ, 431, L9
Mo H. J., Mao S., White S. D. M., 1998, MNRAS, 295, 319
Mortlock D. J., et al., 2011, Nature, 474, 616
Muñoz-Cuartas J. C., Macciò A. V., Gottlöber S., Dutton A. A., 2011, MNRAS, 411, 584
Naab T., Burkert A., 2003, ApJ, 597, 893
O'Shea B. W., Norman M. L., 2007, ApJ, 654, 66
Omukai K., Tsuribe T., Schneider R., Ferrara A., 2005, ApJ, 626, 627
Pacucci F., Volonteri M., Ferrara A., 2015, MNRAS, 452, 1922
Page M. J., Simpson C., Mortlock D. J., Warren S. J., Hewett P. C., Venemans B. P., McMahon R. G., 2014, MNRAS, 440, L91
Pelupessy F. I., Di Matteo T., Ciardi B., 2007, ApJ, 665, 107
Planck Collaboration et al., 2014, A&A, 571, A1
Richards G. T., et al., 2006, ApJS, 166, 470
Richstone D., et al., 1998, Nature, 395, A14
Sani E., Marconi A., Hunt L. K., Risaliti G., 2011, MNRAS, 413, 1479
Sądowski A., 2009, ApJS, 183, 171
Sądowski A., Narayan R., 2016, MNRAS, 456, 3929
Sądowski A., Narayan R., Penna R., Zhu Y., 2013, MNRAS, 436, 3856
Schneider R., Ferrara A., Natarajan P., Omukai K., 2002, ApJ, 571, 30
Schneider R., Ferrara A., Salvaterra R., Omukai K., Bromm V., 2003, Nature, 422, 869
Schneider R., Omukai K., Limongi M., Ferrara A., Salvaterra R., Chieffi A., Bianchi S., 2012, MNRAS, 423, L60
Schneider R., Bianchi S., Valiante R., Risaliti G., Salvadori S., 2015, A&A, 579, A60
Schnittman J. D., Buonanno A., van Meter J. R., Baker J. G., Boggs W. D., Centrella J., Kelly B. J., McWilliams S. T., 2008, Phys. Rev. D, 77, 044031
Shakura N. I., Sunyaev R. A., 1973, A&A, 24, 337
Shapiro S. L., 2005, ApJ, 620, 59
Shen S., Mo H. J., White S. D. M., Blanton M. R., Kauffmann G., Voges W., Brinkmann J., Csabai I., 2003, MNRAS, 343, 978
Silk J., Rees M. J., 1998, A&A, 331, L1
Springel V., 2000, MNRAS, 312, 859
Sutherland R. S., Dopita M. A., 1993, ApJS, 88, 253
Tanaka T., Haiman Z., 2009, ApJ, 696, 1798
Turk M. J., Abel T., O'Shea B., 2009, Science, 325, 601
Valiante R., Schneider R., Salvadori S., Bianchi S., 2011, MNRAS, 416, 1916
Valiante R., Schneider R., Maiolino R., Salvadori S., Bianchi S., 2012, MNRAS, 427, L60
Valiante R., Schneider R., Salvadori S., Gallerani S., 2014, MNRAS, 444, 2442
Valiante R., Schneider R., Volonteri M., Omukai K., 2016, MNRAS
Venemans B. P., et al., 2015, MNRAS, 453, 2259

Volonteri M., 2010, A&A Rev., 18, 279
Volonteri M., Rees M. J., 2005, ApJ, 633, 624
Volonteri M., Rees M. J., 2006, ApJ, 650, 669
Volonteri M., Haardt F., Madau P., 2003, ApJ, 582, 559
Volonteri M., Silk J., Dubus G., 2015, ApJ, 804, 148
Walter F., Carilli C., Bertoldi F., Menten K., Cox P., Lo K. Y., Fan X., Strauss M. A., 2004, ApJ, 615, L17
Wang R., et al., 2010, ApJ, 714, 699
Wang R., et al., 2013, ApJ, 773, 44
Willott C. J., et al., 2007, AJ, 134, 2435
Willott C. J., Bergeron J., Omont A., 2015, ApJ, 801, 123
Yoo J., Miralda-Escudé J., 2004, ApJ, 614, L25
Zubovas K., King A., 2012, ApJ, 745, L34
Zubovas K., King A. R., 2014, MNRAS, 439, 400
de Bennassuti M., Schneider R., Valiante R., Salvadori S., 2014, MNRAS, 445, 3039